J. Fluid Mech. (2005), *vol.* 539, *pp.* 113–135. © 2005 Cambridge University Press
doi:10.1017/S0022112005005458 Printed in the United Kingdom

Moffatt eddies in the cone

By P. N. SHANKAR

Computational and Theoretical Fluid Dynamics Division, National Aerospace Laboratories, Bangalore 560 017, India†
pn_shankar55@rediffmail.com

(Received 15 July 2004 and in revised form 14 February 2005)

Consider Stokes flow in a cone of half-angle α filled with a viscous liquid. It is shown that in spherical polar coordinates there exist similarity solutions for the velocity field of the type $r^{\lambda}\boldsymbol{f}(\theta;\lambda)\exp \mathrm{i}m\phi$ where the eigenvalue λ satisfies a transcendental equation. It follows, by extending an argument given by Moffatt (1964*a*), that if the eigenvalue λ is complex there will exist, associated with the corresponding vector eigenfunction, an infinite sequence of eddies as $r \to 0$. Consequently, provided the principal eigenvalue is complex and the driving field is appropriate, such eddy sequences will exist. It is also shown that for each wavenumber m there exists a critical angle α^* below which the principal eigenvalue is complex and above which it is real. For example, for $m = 1$ the critical angle is about 74.45°. The full set of real and complex eigenfunctions, the inner eigenfunctions, can be used to compute the flow in a cone given data on the lid. There also exist outer eigenfunctions, those that decay for $r \to \infty$, and these can be generated from the inner ones. The two sets together can be used to calculate the flow in a conical container whose base and lid are spherical surfaces. Examples are given of flows in cones and in conical containers which illustrate how α and r_0, a length scale, affect the flow fields. The fields in conical containers exhibit toroidal corner vortices whose structure is different from those at a conical vertex; their growth and evolution to primary vortices is briefly examined.

1. Introduction

We address here two issues concerning slow steady viscous flows, namely the existence of corner eddies in three-dimensional flows and the analytic description of such three-dimensional flows in confined geometries. Ever since Moffatt's (1964*a*) discovery, that in general, in a plane flow involving corners, there exists an infinite sequence of eddies as the corners are approached, there has been considerable interest in whether a similar result is true in three-dimensions. It has proved difficult to reach a clear unambiguous answer to this question. In part this may be due to the possibility that the wrong generalizations have been sought; in part it may be due to the possibility that the situation is altogether more complex in this case. For example, confined streamlines are in general closed in two-dimensions while they are not necessarily so in three-dimensions; whereas only simple centres and saddles can be stagnation points in the former, the situation is much more complicated in the latter. Sano & Hasimoto (1980), Moffatt & Mak (1999) and Shankar (2000) all consider a three-dimensional wedge type of geometry for the corner. All of these analyses conclude that an infinite sequence of eddies exist for flows that are antisymmetric in a certain sense whereas

† Present address: 33/1 Kasturba Road Cross, Bangalore 560 001, India.

https://doi.org/10.1017/S0022112005005458 Published online by Cambridge University Press

such sequences do not exist in the corresponding symmetric cases (A section of Hills & Moffatt (2000) deals with an approximate analysis of the corner problem. The paper is valuable also for its results from experimental flow visualization which suggest the existence of closed streamlines.). Yet none of these works are totally satisfactory and this not just because of the approximations and assumptions that must be made. Our unease stems from the fact the these results do not follow naturally and easily as they do in Moffatt (1964a) where a similarity solution leads to an eigenvalue problem with complex eigenvalues. In fact, no exact simple similarity solution was found in these three-dimensional cases.

It is only recently that the natural extension of Moffatt (1964*a*) to three dimensions was suggested in Malyuga (2005), who considered the flow in an infinite cone generated by prescribed data on a finite ring along the conical sidewall. This type of motion, that could be considered to model the flow generated by finite belts or sleeves inserted in the conical wall, corresponds exactly to Moffatt (1964*b*). In this work, Moffatt not only demonstrated an example of a field where the infinite sequence of eddies existed, but also determined their strengths exactly, something which the earlier similarity analysis could not yield. Malyuga (2005) shows, for the type of flow field that he considers, the existence of corner eddies at the vertex for all azimuthal wavenumbers m. We see here a difference from the wedge cases considered above, and a closer connection to the planar geometry; thus the conical vertex seems the natural extension of the plane corner. Malyuga's work, which is an extension of Moffatt (1964*b*), indicates the possibility of an extension to Moffatt (1964*a*). That is, a simple, direct similarity solution which can be used to predict the local behaviour at the vertex. This exists in Malyuga (2005), but is hidden by the analytical machinery used such as the Mellin transform. Thus, one of the motivations here is to provide a simple similarity solution for flow in the cone from which the general behaviour near the vertex can be deduced as in Moffatt (1964*a*).

The second of the two issues that we are concerned with is the analysis of three-dimensional internal flows in containers. While there is a vast literature on two-dimensional internal flows, often concerned with 'lid-driven cavity flows', and a much smaller, but still significant, literature on three-dimensional external Stokes flows past bodies, there is little work on three-dimensional internal flows. There are many applications where such flows are important and the only reason for the paucity is that the analysis presents special difficulties. Not only are the fields genuinely vector fields, but there are also problems in satisfying the boundary conditions. It appears that Shankar (1997), dealing with flow in a cylinder, was the first fully three-dimensional internal Stokes flow analysis available. For an analysis of the same problem by the superposition method see Meleshko, Malyuga & Gomilko (2000). To date there is no other geometry for which we have such analytical solutions. Thus, our second purpose is to develop a fully three-dimensional analysis for internal flows in conical containers whose top and bottom walls are spherical. The special features of the flow fields are: (i) they depend on two parameters, the cone angle and the radial dimension, rather than just one, the height, in the cylinder; (ii) the transition from the cone to the conical container involves a change from a pure corner vortex field at the vertex to a more complicated corner field along the curving bottom corner; and (iii) the boundaries now involve curvature along two directions rather than just one as in the cylinder.

As in our earlier papers (Shankar 1997, 1998), we will develop a solution procedure based on complex eigenfunction expansions and the method of least squares to determine the expansion coefficients.

https://doi.org/10.1017/S0022112005005458 Published online by Cambridge University Press

2. Analysis

We consider slow viscous flow in a cone of circular section and cone angle 2α. Suitably normalized, the governing Stokes flow equations are

$$\nabla \cdot \boldsymbol{u} = 0, \quad \nabla p = \nabla^2 \boldsymbol{u}, \tag{1a, b}$$

where $\boldsymbol{u}$ is the velocity field and p is the pressure. We will assume throughout that the velocity must, by the no-slip condition, vanish on the cone. To begin with, we will find similarity solutions to (1) which satisfy this condition on the cone and, as a consequence, be able to deduce the nature of the eddy structure in the neighbourhood of the vertex for essentially arbitrary conditions in the far field. The similarity solutions are the 'inner eigenfunctions' which vanish at the vertex of the cone. These eigenfunctions can be used to represent flows in a cone where the flow is driven by the motion of the lid of the cone, assumed to be spherical. We will then show that there exist a set of 'outer eigenfunctions' which decay for large radial distances from the vertex. Using both sets of eigenfunctions, we can analyse the flow in a conical container where data is prescribed on the spherical top and bottom walls.

2.1. *Similarity solutions and the inner eigenfunctions*

We wish to find solutions to the field equations (1) which satisfy the no-slip boundary conditions on the cone. Let (r, θ, ϕ) be a spherical coordinate system with origin at the vertex of the cone and with the symmetry axis lying on $\theta = 0$ where θ is the polar angle. Thus, the no-slip boundary condition must apply on $\theta = \alpha$ for all r if the cone is infinite, or over a finite length if it is finite. For reasons that have been explained in earlier papers it will be convenient to derive solutions to (1) using the representation (Imai 1973; Tran-Cong & Blake 1982)

$$\boldsymbol{v} = \nabla(\boldsymbol{r} \cdot \boldsymbol{A} + B) - 2\boldsymbol{A}, \tag{2a}$$

$$p = 2\nabla \cdot \boldsymbol{A}. \tag{2b}$$

It can be shown that if B and $\boldsymbol{A} = (A_r, A_\theta, A_\phi)$ are solutions of the scalar and vector Laplace equations, respectively, i.e. if

$$\nabla^2 B = \frac{1}{r^2}\frac{\partial}{\partial r}\left(r^2 \frac{\partial B}{\partial r}\right) + \frac{1}{r^2 \sin\theta}\frac{\partial}{\partial \theta}\left(\sin\theta \frac{\partial B}{\partial \theta}\right) + \frac{1}{r^2 \sin^2\theta}\frac{\partial^2 B}{\partial \phi^2} = 0, \tag{3a}$$

$$\begin{aligned}\nabla^2 \boldsymbol{A} = {} & \boldsymbol{e}_r \left\{\nabla^2 A_r - \frac{2A_r}{r^2} - \frac{2}{r^2 \sin\theta}\frac{\partial}{\partial \theta}(\sin\theta A_\theta) - \frac{2}{r^2 \sin\theta}\frac{\partial A_\phi}{\partial \phi}\right\} \\ & + \boldsymbol{e}_\theta \left\{\nabla^2 A_\theta + \frac{2}{r^2}\frac{\partial A_r}{\partial \theta} - \frac{A_\theta}{r^2 \sin^2\theta} - \frac{2\cos\theta}{r^2 \sin^2\theta}\frac{\partial A_\phi}{\partial \phi}\right\} \\ & + \boldsymbol{e}_\phi \left\{\nabla^2 A_\phi + \frac{2}{r^2 \sin\theta}\frac{\partial A_r}{\partial \phi} + \frac{2\cos\theta}{r^2 \sin^2\theta}\frac{\partial A_\theta}{\partial \phi} - \frac{A_\phi}{r^2 \sin^2\theta}\right\} = 0,\end{aligned} \tag{3b}$$

then the field $\{\boldsymbol{v}, p\}$ given by (2) will satisfy the Stokes equations (1). It may be noted that the components of $\boldsymbol{A}$ satisfy coupled variable coefficient equations. Also, since there are three scalar boundary conditions to be satisfied on the cone, we require three independent fields to satisfy them. The idea then is to find a scalar field B satisfying (3*a*) and two vector fields $\boldsymbol{A}$ satisfying (3*b*) and them combine them appropriately to satisfy the no-slip condition on the cone. Since the coefficients in (3) are all independent of the azimuthal angle ϕ, it is natural to seek solution fields whose ϕ-dependence is of the form $\exp im\phi$, where the integer m is the azimuthal wavenumber. Linearity then permits superposition with m ranging over all the integers.

https://doi.org/10.1017/S0022112005005458 Published online by Cambridge University Press

(i) For the scalar field we choose the standard form of the separable solution to Laplace's equation in spherical coordinates

$$B(r,\theta,\phi;\nu) = r^{\nu} \mathrm{e}^{\mathrm{i}m\phi} P_{\nu}^{m}(\cos\theta) \tag{4}$$

where $P_{\nu}^{m}(x)$ is the associated Legendre function of order m, degree ν and with argument x (see Appendix A).

(ii) It is pointed out in Morse & Feshbach (1953) that $\boldsymbol{M} = \boldsymbol{e}_r \times \nabla(rB)$ with B given by (4) is a solution of the vector Laplace equation (3*b*). We therefore choose for the first vector field $\boldsymbol{A}_1$

$$\boldsymbol{A}_1(r,\theta,\phi;\nu) = -r^{\nu} \mathrm{e}^{\mathrm{i}m\phi} \left\{ \frac{m}{\sin\theta} P_{\nu}^{m}(\cos\theta)\boldsymbol{e}_{\theta} + \mathrm{i} P_{\nu}^{m'}(\cos\theta)\boldsymbol{e}_{\phi} \right\}. \tag{5}$$

Here and in what follows, primes always indicate differentiation with respect to θ, i.e. $P_{\nu}^{m'}(\cos\theta) = \mathrm{d}P_{\nu}^{m}(\cos\theta)/\mathrm{d}\theta$. It may be checked from (2*a*) that the vector field $\boldsymbol{A}_1$ yields a velocity field that has no radial component.

(iii) For an independent second vector field, we note that $B(r,\theta,\phi;\nu)\boldsymbol{e}$, where $\boldsymbol{e}$ is one of the unit vectors in the corresponding Cartesian coordinate frame, satisfies (3*b*). We therefore set

$$\boldsymbol{A}_2(r,\theta,\phi;\nu) = r^{\nu} \mathrm{e}^{\mathrm{i}m\phi} P_{\nu}^{m}(\cos\theta)\boldsymbol{e}_k = r^{\nu} \mathrm{e}^{\mathrm{i}m\phi} \left\{ \cos\theta\, P_{\nu}^{m}(\cos\theta)\boldsymbol{e}_r - \sin\theta\, P_{\nu}^{m}(\cos\theta)\boldsymbol{e}_{\theta} \right\}. \tag{6}$$

Before proceeding further, it will prove convenient to write down the general field as a sum of fields that are symmetric about $\phi = 0$, i.e. those in which v_r and v_θ are symmetric in ϕ, and those that are antisymmetric. Here we will only consider the former, with the clear understanding that the latter can be handled in an identical way and the general field will be a superposition of the two. Thus, in what follows, we will only take the appropriate parts of the fields derived above.

Now it is necessary to take a linear combination of (i), (ii) and (iii) such that the no-slip condition is satisfied on the cone, i.e. on $\theta = \alpha$. To this end, we add a units of $\boldsymbol{A}_1(r,\theta,\phi;\nu)$ and b units of $\boldsymbol{A}_2(r,\theta,\phi;\nu)$ to one unit of $B(r,\theta,\phi;\nu+1)$ and evaluate the velocity field on the cone from (2*a*). Since this has to vanish for all r and ϕ we have

$$v_r(r,\alpha,\phi;\nu) = r^{\nu}\cos m\phi \left[(\nu+1) P_{\nu+1}^{m}(\cos\alpha) + b(\nu-1)\cos\alpha\, P_{\nu}^{m}(\cos\alpha) \right] = 0, \tag{7a}$$

$$v_\theta(r,\alpha,\phi;\nu) = r^{\nu}\cos m\phi \left[P_{\nu+1}^{m'}(\cos\alpha) + a\frac{2m}{\sin\alpha} P_{\nu}^{m}(\cos\alpha) + b\left\{ \sin\alpha\, P_{\nu}^{m}(\cos\alpha) + \cos\alpha\, P_{\nu}^{m'}(\cos\alpha) \right\} \right] = 0, \tag{7b}$$

$$v_\phi(r,\alpha,\phi;\nu) = -r^{\nu}\sin m\phi \left[\frac{m}{\sin\alpha} P_{\nu+1}^{m}(\cos\alpha) + 2a\, P_{\nu}^{m'}(\cos\alpha) + b\, m\cot\alpha\, P_{\nu}^{m}(\cos\alpha) \right] = 0. \tag{7c}$$

In order for this system to have a non-trivial solution, it is necessary that ν satisfy the characteristic equation

$$\mathscr{E}(\nu) = -\frac{2m^2\cot\alpha}{\sin\alpha} P_{\nu}^{m\,2} P_{\nu+1}^{m} + (\nu+1) P_{\nu+1}^{m} P_{\nu}^{m'} \left(\sin\alpha\, P_{\nu}^{m} + \cos\alpha\, P_{\nu}^{m'} \right) - (\nu-1)\cos\alpha\, P_{\nu+1}^{m'} P_{\nu}^{m'} P_{\nu}^{m} = 0, \tag{8}$$

where it is understood that the argument of the associated Legendre functions is everywhere $\cos\alpha$ and, as pointed out earlier, the primes indicate differentiation with

https://doi.org/10.1017/S0022112005005458 Published online by Cambridge University Press

j	μ_j	λ_j
$\alpha = 10°$		
1	29.97537	14.25128 + 6.37344i
2	48.39658	33.91133 + 9.14973i
3	66.56760	52.40078 + 10.34172i
4	84.66201	70.64367 + 11.16256i
5	102.72220	88.78899 + 11.79204i
$\alpha = 20°$		
1	14.75253	6.93415 + 3.09821i
2	23.95741	16.72614 + 4.48285i
3	33.04042	25.96367 + 5.08033i
4	42.08621	35.08182 + 5.49143i
5	51.11541	44.15263 + 5.80661i
$\alpha = 30°$		
1	9.68519	4.52119 + 1.96325i
2	15.81526	11.00731 + 2.88265i
3	21.86777	17.15751 + 3.28269i
4	27.89669	23.23255 + 3.55756i
5	33.91512	29.27763 + 3.76818i
$\alpha = 45°$		
1	6.31651	2.94546 + 1.14074i
2	10.39292	7.20800 + 1.74947i
3	14.42349	11.29538 + 2.01908i
4	18.44028	15.33953 + 2.20366i
5	22.45095	19.36625 + 2.34489i
$\alpha = 160°$		
1	0.22255	2.36165 + 0.10970i
2	1.15445	3.49676 + 0.18667i
3	1.30342	4.62936 + 0.24701i
4	2.00365	5.75770 + 0.29810i
5	3.01679	6.88231 + 0.34135i

TABLE 1. The first five real and complex eigenvalues when the azimuthal wavenumber $m = 1$.

respect to θ. If $\nu = \lambda$ is a solution of (8), then a and b are given by

$$a = -\frac{\sin\alpha}{2m P_\lambda^m}\left[P_{\lambda+1}^{m'} + \left\{\sin\alpha P_\lambda^m + \cos\alpha P_\lambda^{m'}\right\} b\right], \quad b = -\frac{(\lambda+1)P_{\lambda+1}^m}{(\lambda-1)\cos\alpha P_\lambda^m}, \qquad (9a, b)$$

and the velocity field given by $\boldsymbol{v}(r, \theta, \phi; \lambda)$ is a similarity solution of the Stokes equations that satisfies the no-slip conditions on the cone. Note that (8) is analogous to equation (3.1) of Malyuga (2005) and must lead to the same eigenvalues.

Using Newton's method in conjunction with the principle of the argument and standard continuation techiques, we can easily find the roots of (8) which have a positive real part. Calculations show that for each $m > 0$ and α there exists a complex sequence of roots $\{\lambda_j = \lambda_j^r + i\lambda_j^i,\ j = 1, 2, \ldots\}$ and a purely real sequence of roots $\{\mu_j, j = 1, 2, \ldots\}$ where the ordering is by the magnitude of the real part. Note that the conjugate of λ_j is also a root of (8). Table 1 gives the first five roots of each sequence for a number of values of the cone half-angle α when the azimuthal wavenumber $m = 1$, the most important case; table 2 gives similar data for the $m = 2$ case. We note that for given α, both $(\mu_{j+1} - \mu_j)$ and $(\lambda_{j+1}^r - \lambda_j^r)$ tend to constants as $j \to \infty$, a fact that is of use in obtaining the roots. This also suggests that the roots have asymptotic forms for large j that can be derived from (8) using the asymptotic

https://doi.org/10.1017/S0022112005005458 Published online by Cambridge University Press

j	μ_j	λ_j
$\alpha = 10^\circ$		
1	37.76093	21.97942 + 7.45914i
2	56.58463	42.01197 + 9.75931i
3	74.95021	60.73346 + 10.78397i
4	93.16209	79.11690 + 11.51512i
5	111.30160	97.35840 + 12.09160i
$\alpha = 20^\circ$		
1	18.66259	10.81617 + 3.64198i
2	28.06355	20.79091 + 4.78673i
3	37.24110	30.14061 + 5.30060i
4	46.34390	39.32674 + 5.66693i
5	55.41154	48.44406 + 5.95560i

TABLE 2. The first five real and complex eigenvalues when the azimuthal wavenumber $m = 2$.

m	μ_1	λ_1
0		7.91093 + 2.81640i
1	9.68519	4.52120 + 1.96325i
2	12.31152	7.12971 + 2.32671i
3	14.82863	9.56271 + 2.58250i
4	17.27702	11.91093 + 2.78805i
5	19.67690	14.20715 + 2.96310i

TABLE 3. The real and complex eigenvalues with smallest real part for $0 \leqslant m \leqslant 5$, $\alpha = 30^\circ$.

form of P_λ^m for large λ. However, in view of the algebraic complexity involved and the unsuitability of such a formula for our purposes (where it is the smallest roots that are important and these have to be computed directly) we have not derived this asymptotic formula. For a given cone half-angle $\alpha = 30^\circ$, the principal eigenvalues for $0 \leqslant m \leqslant 5$ are given in table 3. Noted that the $m = 1$ mode is dominant and this is true for all angles.

Since the axisymmetric case, $m = 0$, involves only two components of velocity, it has to be handled separately. We now add b units of $\boldsymbol{A}_2$ to one of B and now require v_r and v_θ to vanish on the cone. This procedure leads to the characteristic equation

$$(\nu + 1) P_{\nu+1} \{\sin\alpha P_\nu + \cos\alpha P'_\nu\} - (\nu - 1)\cos\alpha P_\nu P'_{\nu+1} = 0, \tag{10}$$

while the scalar b is now given by

$$b = -\frac{(\lambda + 1) P_{\lambda+1}}{(\lambda - 1)\cos\alpha\, P_\lambda}. \tag{11}$$

For each α there exists only one complex sequence $\{\lambda_j, j = 1, 2 \ldots\}$ of solutions to (10). This is entirely consistent with the notion that the type and number of real sequences is determined by the number of boundary conditions that would have to be satisfied by such sequences: in this case since only two components v_r and v_θ can be prescribed on a spherical end surface, only one complex sequence (or two real ones) can exist. In this paper, we will not consider in any depth the axisymmetric $m = 0$ case, where the roots are purely complex for sufficiently small cone angle, as this case

https://doi.org/10.1017/S0022112005005458 Published online by Cambridge University Press

is two-dimensional and is of little interest. However, we can refer to Wakiya (1976), Liu & Joseph (1978) and Weidman & Calmidi (1999) for related axisymmetric work.

2.2. *Moffatt eddies*

The fact that similarity solutions exist, as shown in § 2.1, suggests that an infinite sequence of eddies may exist in the neighbourhood of the vertex of the cone. If the eigenfunction sequences that we have derived are complete, no matter how the field is generated in the far field, we may expect the field in the neighbourhood of the vertex to have the representation

$$\boldsymbol{u}(r,\theta,\phi) \sim \mathrm{Re}\sum_{m=0}^{\infty} \mathrm{e}^{\mathrm{i}m\phi} \sum_{j=1}^{\infty} \{a_j r^{\mu_j} \boldsymbol{f}_j(\theta;\mu_j) + b_j r^{\lambda_j} \boldsymbol{g}_j(\theta;\lambda_j)\}, \tag{12}$$

where $\boldsymbol{f}_j(\theta;\mu_j)$ is the real velocity vector eigenfunction corresponding to μ_j, and $\boldsymbol{g}_j(\theta;\lambda_j)$ is the complex velocity vector eigenfunction corresponding to λ_j, and the a_j and b_j are scalars that are determined by the far field. Of course, the eigenvalues and eigenfunctions depend on the azimuthal wavenumber m, but this dependence, in order to reduce the clutter, has not been shown in (12). It is clear from the form of the expansion that for $r \to 0$, the field will be dominated by the term which contains the eigenvalue with the smallest real part, i.e. the dominant one. Hence in the following analysis, we will only consider a single term of the above sum, the one containing the dominant eigenvalue. For the moment, let us assume that it is λ_1 which is complex and that the field is symmetric in ϕ as in (7).

While we wish to follow the argument that has become standard since Moffatt (1964*a*), a little more care is required here. Whereas in Moffatt (1964*a*) the field was planar, all streamlines away from the boundary were closed and the only stagnation points were centres or saddles, the situation in the three-dimensional field considered here is considerably more complex. In fact, the very definition of an eddy is now uncertain since the three-dimensional streamlines may not even be closed in general. To appreciate better the nature of the fields considered here, we first write down the complex velocity field associated with the principal eigenvalue λ, where we have dropped the subscript 1,

$$v_r(r,\theta,\phi;\lambda) = r^{\lambda}\cos m\phi\left[(\lambda+1)P_{\lambda+1}^{m} + b(\lambda-1)\cos\theta\, P_{\lambda}^{m}\right], \tag{13a}$$

$$v_\theta(r,\theta,\phi;\lambda) = r^{\lambda}\cos m\phi\left[P_{\lambda+1}^{m'} + a\frac{2m}{\sin\theta}P_{\lambda}^{m} + b\left\{\sin\theta\, P_{\lambda}^{m} + \cos\theta\, P_{\lambda}^{m'}\right\}\right], \tag{13b}$$

$$v_\phi(r,\theta,\phi;\lambda) = -r^{\lambda}\sin m\phi\left[\frac{m}{\sin\theta}P_{\lambda+1}^{m} + 2a\,P_{\lambda}^{m'} + b\,m\cot\theta\, P_{\lambda}^{m}\right]. \tag{13c}$$

Here the argument of all the associated Legendre functions is understood to be $\cos\theta$. The following observations may be made.

(*a*) For all integers m, the field is symmetric about $\phi = 0$ in the sense that v_r and v_θ are symmetric about this plane while v_ϕ is antisymmetric.

(*b*) For all m, the azimuthal velocity v_ϕ vanishes in the plane $\phi = 0, \pi$. This implies that for all m, the streamlines in this plane remain in this plane and are planar. However, their features are three-dimensional.

(*c*) For all $m > 1$, $P_{\lambda}^{m}(x) \to 0$ as $x \to 1$. We therefore conclude from (13*a*) that $v_r \to 0$ as $\theta \to 0$.

(*d*) From (*a*) and (*c*), the only component that can be non-zero on the polar axis $\theta = 0$ in the plane $\phi = 0, \pi$ is v_θ. However, this has to be continuous across this axis. Note that in (13*b*), $\cos m\phi$ changes sign as ϕ switches from 0 to π if m is odd, but

https://doi.org/10.1017/S0022112005005458 Published online by Cambridge University Press

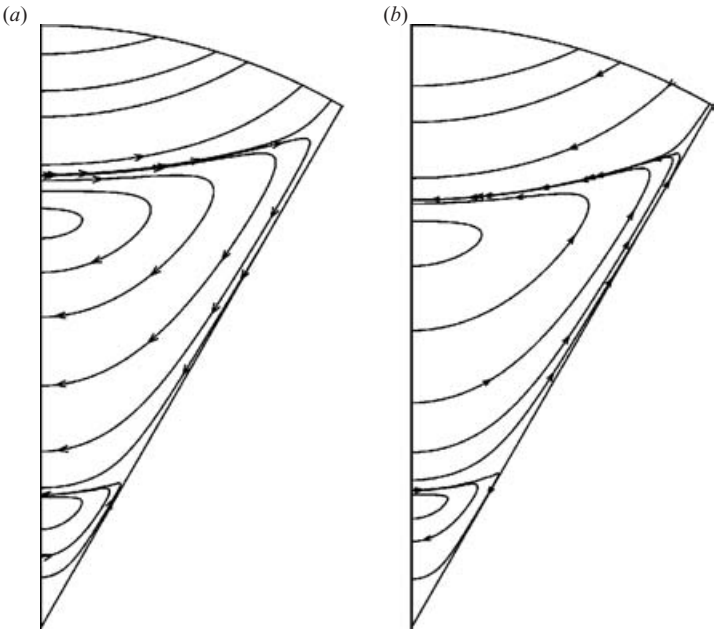


FIGURE 1. The velocity fields generated by the principal vector eigenfunctions in the symmetry plane $\phi = 0$. Cone half-angle $\alpha = 30°$. (*a*) A typical antisymmetric case $m = 3$, and (*b*) a typical symmetric case $m = 4$. Note that the radial upper boundary is not a solid boundary and is only meant to limit the figure.

not if m is even. This implies that $v_\theta \to 0$ as $\theta \to 0$ if m is even. In other words, the polar axis is a stagnation line for even $m \geqslant 2$.

(*e*) For m even, $v_\phi = 0$ on the plane $\phi = \pi/2,\ 3\pi/2$. Thus, for m even, the field is also symmetric about the plane $\phi = \pi/2$, while for odd m it is antisymmetric. Moreover, the streamlines in this plane remain in this plane for even m.

These observations, together with the streamline plots in the symmetry plane $\phi = 0$ shown in figure 1, will help us to appreciate better the nature of the basic fields generated by the principal vector eigenfunctions. Figure 1(*a*) shows the streamlines in the symmetry plane for $m = 3$, a typical odd wavenumber, while figure 1(*b*) is for a typical even wavenumber, $m = 4$; the cone is of half-angle $\alpha = 30°$. Note that the streamlines have been generated by taking the real parts of (13*a*) and (13*b*). Superficially, the two figures look very much alike, but this impression is misleading. Because the $m = 3$ field is antisymmetric about $\phi = \pi/2$, the streamlines actually cross the polar axis with, in general, non-zero v_θ and form closed streamline patterns with stagnation points on the polar axis. On the other hand, the $m = 4$ field is symmetric about $\phi = \pi/2$ and the polar axis is a stagnation line. Therefore the streamlines seen in figure 1(*b*) start on the polar axis, which is a stagnation line, and just return to it. With this understanding of the flow in the symmetry plane one can by continuation, together with observations (*a*) to (*e*), see what the flow field will look like away from this plane.

We are now in a position to look into the question of the existence of eddies near the vertex of the cone essentially using the argument given in Moffatt (1964*a*). From the discussion above, it appears that we would best examine the field in the plane $\phi = 0, \pi$ for reversals in the direction of one component of velocity; a similar argument

https://doi.org/10.1017/S0022112005005458 Published online by Cambridge University Press

could then be applied to other planes to suggest the existence or otherwise of an infinite sequence of eddies. Let us first consider the case of odd $m \geqslant 1$. In this case, from (13*b*), the velocity component $v_\theta(r, \theta, 0; \lambda_1)$ in the plane $\phi = 0$ takes the form

$$v_\theta(r, \theta, 0; \lambda_1) = (a + \mathrm{i}b)\left(\frac{r}{r_0}\right)^{\lambda_1}, \tag{14}$$

where a and b are real scalars and r_0 is a real scale factor that is arbitrary here and in practice will be determined by the far field. Let $\lambda_1 = p_1 + \mathrm{i}q_1$; then a short calculation shows that $(r/r_0)^{\lambda_1} = (r/r_0)^{p_1}[\cos(q_1 \ln(r/r_0)) + \mathrm{i}\sin(q_1 \ln(r/r_0))]$ and hence that

$$\mathrm{Re}\left[\left(\frac{r}{r_0}\right)^{\lambda_1}(a + \mathrm{i}b)\right] = \gamma\left(\frac{r}{r_0}\right)^{p_1}\sin\left(q_1 \ln\frac{r}{r_0} + \epsilon\right), \tag{15}$$

where γ and ϵ are real. It may be observed that as $r \to 0$, $\ln(r/r_0) \to -\infty$ and so the sign of the right-hand side of (15) changes repeatedly as $r \to 0$; in other words, the real part of $v_\theta(r, \theta, 0; \lambda_1)$ changes sign infinitely often as the vertex is approached. Since all the streamlines are closed in this plane we can infer that the streamline pattern here is the section of an infinite sequence of eddies that exist as the vertex is approached. We can attempt to use the same argument to any other constant ϕ plane, but since the streamlines are not closed in those planes there is some ambiguity in the argument which is not there when $\phi = 0$. A similar argument can be used in the even m case, but now θ has to be bounded away from 0, since the polar axis is a stagnation line. However, the same argument goes through since the streamlines remain in this plane and are essentially closed. In conclusion, Moffatt eddies exist for all m and all α for which the principal eigenvalue is complex. It is also easy to show from (15) that the dimensions of the eddies fall off in a geometrical progression with common ratio $\exp(\pi/q_1)$ while the intensities fall off with common ratio $\exp(\pi p_1/q_1)$.

The most important azimuthal wavenumber is $m = 1$ since it corresponds to the case where the field in the cone is generated by a spherical lid moving uniformly in its surface in one direction, i.e. the case of the lid-driven cone. For this case, figure 2 shows the streamline patterns in the symmetry plane for a number of cone half-angles. In each case, the motion is generated by the motion of the spherical lid. Since these fields will be discussed later, we only wish here to draw attention to the sequences of corner eddies that were deduced to exist. The above arguments imply that in each case the sequence is an infinite one of diminishing size and strength. The corresponding principal eigenvalues can be read off from table 1 and the eddy parameters calculated from them, as shown above. Figure 3(*a*) shows similar streamline patterns for the $m = 2$ case when $\alpha = 20^\circ$ while the relevant principal eigenvalue is given in table 2. In this case too, the flow is driven by an appropriate motion of the lid whose details will be given later. Here the main point of interest is the similarity of figure 3(*a*) to figure 2(*b*) even though the three-dimensional fields are very different. Again the sequence of eddies near the vertex is manifest.

Examining table 1, we observe that both the real and the imaginary parts of λ_1 decrease with increasing α. The question of interest is whether λ_1 can become purely real at some critical α; in this case, the principal eigenvalue will become real and the eddy sequences will cease to exist beyond this angle. Figure 4 shows the trajectories in the complex plane with increasing cone angle of the first two complex eigenvalues. It is clear that λ_1 has to become real at some angle beyond 70° and calculations show that the critical angle α^* is about 74.45°. Thus beyond this critical angle, the principal eigenvalue is real and so the corner eddies no longer exist. The figure also

https://doi.org/10.1017/S0022112005005458 Published online by Cambridge University Press

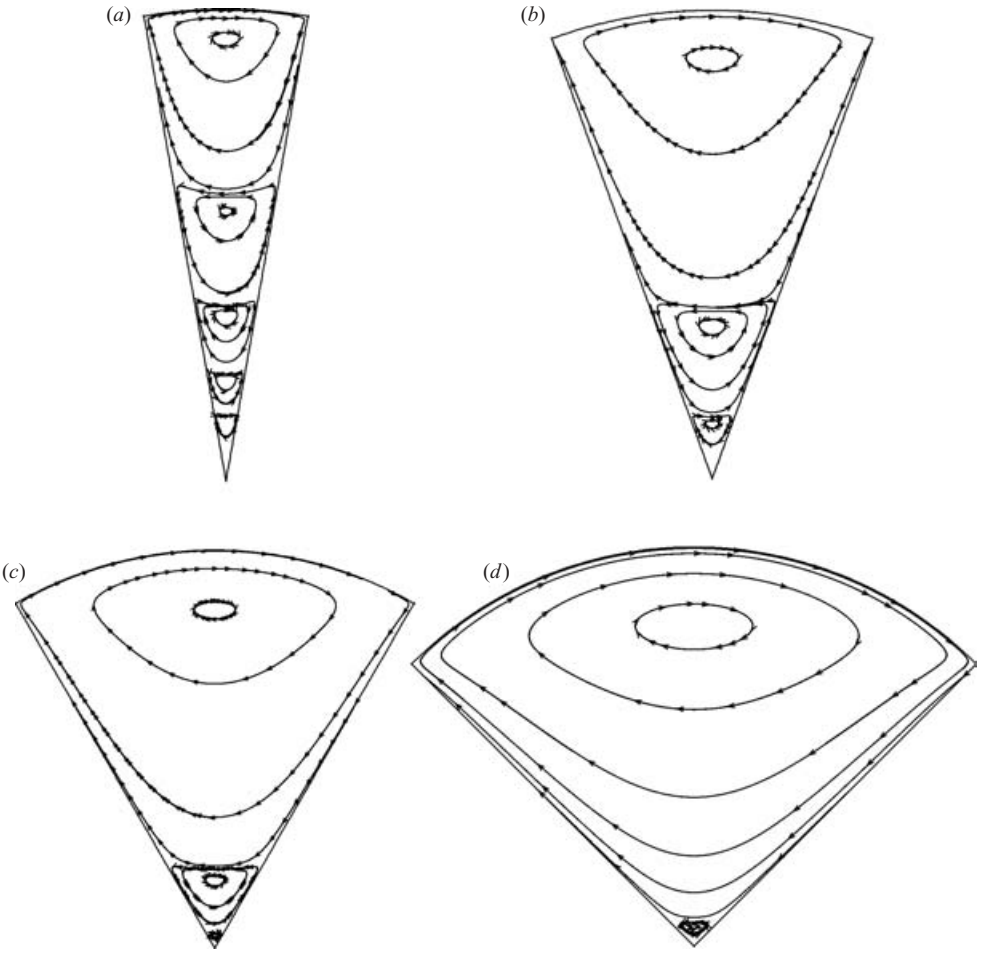


FIGURE 2. The dependence on the cone half-angle of slow viscous flow in conical containers. Streamlines in the symmetry plane $\phi = 0, \pi$ are shown here for the case $m = 1$. (*a*) $\alpha = 10°$, (*b*) 20°, (*c*) 30° and (*d*) 45°.

shows that λ_2 must become real beyond 80° and, in fact, this root becomes real when $\alpha \sim 82.95°$. Now the pattern is clear. As α increases beyond α^*, more and more of the complex eigenvalues become real until at $\alpha = 90°$, when the cone becomes a plane, all the eigenvalues are real. When the cone angle is increased still further, i.e. when the field is that of flow over a conical hill rather than in a cone, complex eigenvalues once again begin to appear†; the only difference now though is that the principal eigenvalue is always real. This can be seen in table 1 where for $\alpha = 160°$, the smallest complex eigenvalue is approximately $2.36 + 0.11\mathrm{i}$ while the principal eigenvalue is real and is about 0.22 and it is this that will dominate near the apex of the inverted cone. Similar conclusions hold for all m.

† For the $m = 0$ case, Liu & Joseph (1978) report, 'All roots are real-valued when $\theta_0 > 90°$', where θ_0 is the cone half-angle. This is incorrect. For example, when $m = 0$ and $\theta_0 = 100°$, the first three complex eigenvalues are approximately $3.081 + 0.187\mathrm{i}$, $4.875 + 0.377\mathrm{i}$ and $6.668 + 0.490\mathrm{i}$, while the principal eigenvalue is about 1.557.

https://doi.org/10.1017/S0022112005005458 Published online by Cambridge University Press

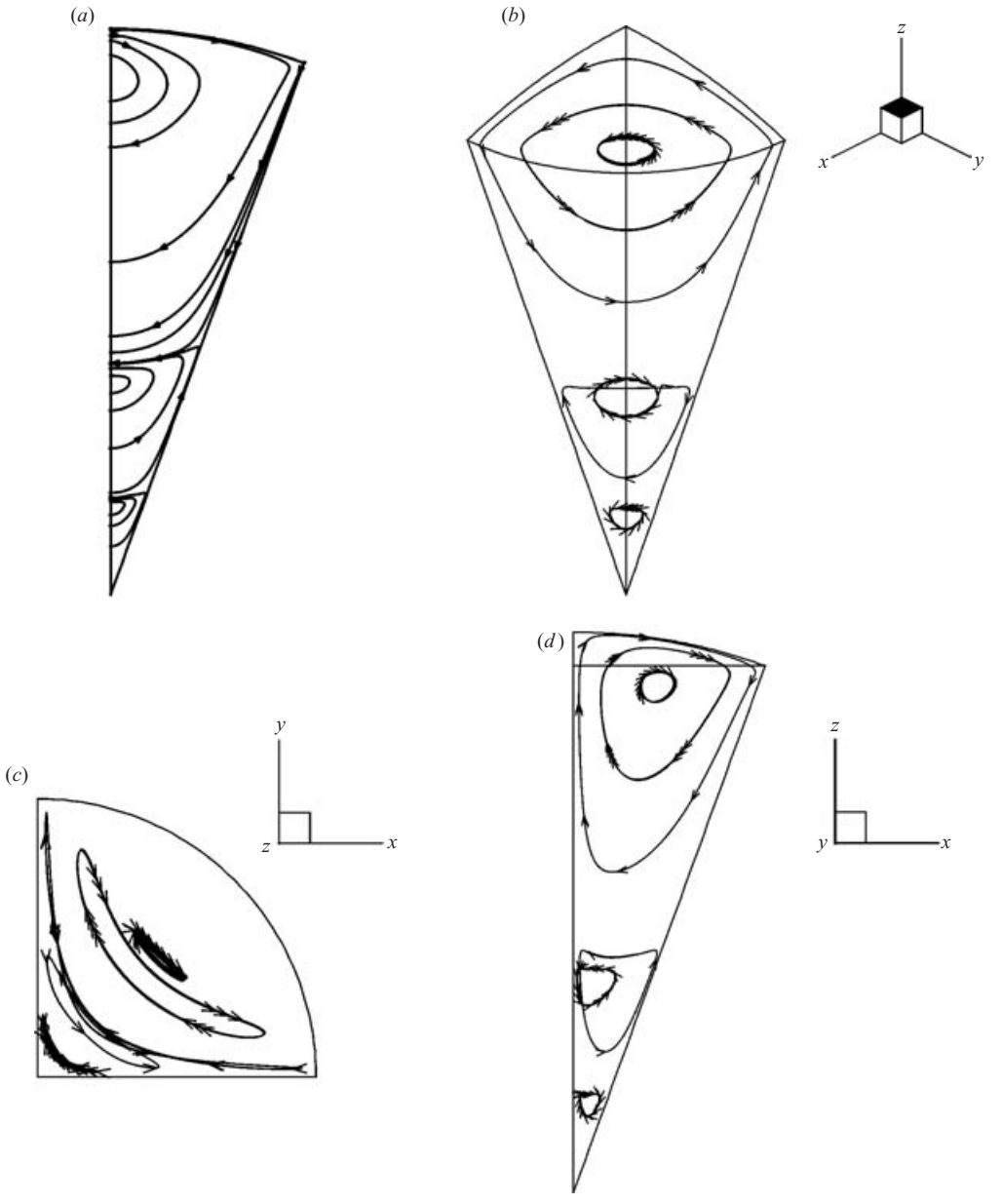


FIGURE 3. The flow field in a cone where the azimuthal wavenumber $m = 2$. Note that the flow field is symmetric about $\phi = 0$ and $\phi = \pi/2$ and so only one quarter of the cone is shown. $\alpha = 20°$. (*a*) Streamlines in the plane $\phi = 0$, (*b*) three-dimensional streamlines seen in perspective, (*c*) as seen in plan and (*d*) as seen in the *y*-direction.

The bifurcation pointed out above actually occurs for all m and this can be seen in figure 5 where either $\mathrm{Re}\lambda_1$ or μ_1 is plotted against α for a number of wavenumbers. In each case, with increasing α, the principal complex eigenvalue λ_1 bifurcates at a critical angle into two real eigenvalues μ_1 and μ_2, with the former becoming the principal eigenvalue. Note that μ_2 is not shown in the figure; for the corresponding wedge case, where both branches are shown, see Moffatt & Duffy (1980). Two important facts

https://doi.org/10.1017/S0022112005005458 Published online by Cambridge University Press

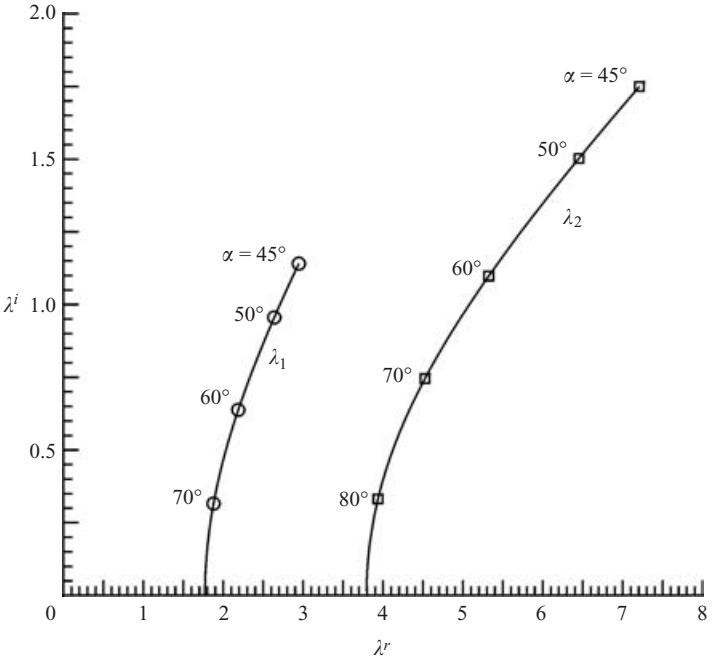


FIGURE 4. The trajectories of the first two complex eigenvalues in the complex λ-plane as the cone half-angle α is increased. $m = 1$. ○, λ_1; □, λ_2.

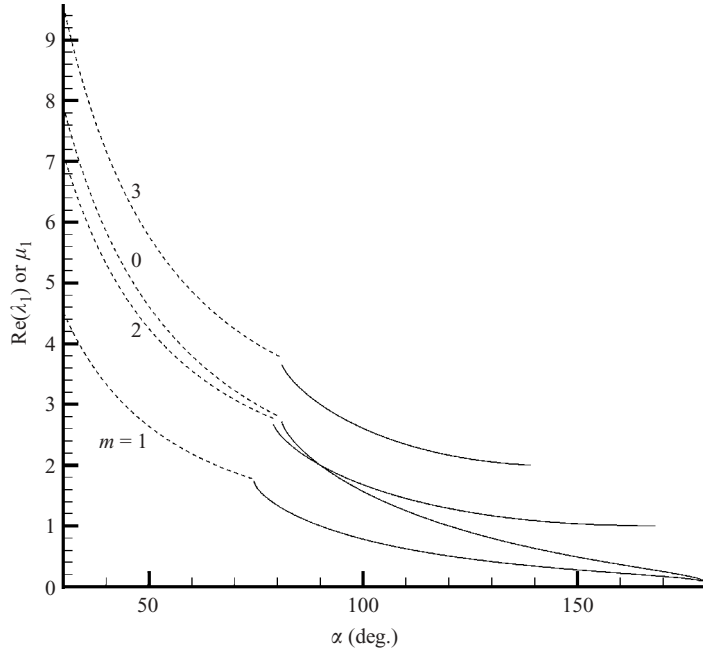


FIGURE 5. The variation of the real part of the principal eigenvalue with the cone half-angle for $m = 0, 1, 2$ and 3. The dotted lines indicate that the real part of λ_1 is plotted while the solid lines indicate μ_1. In each case, the angle at which they join is the critical angle where the bifurcation takes place. Note that the $m = 1$ eigenvalue is dominant over the whole range.

https://doi.org/10.1017/S0022112005005458 Published online by Cambridge University Press

ought to be noted. First, the critical angles for $m=0$ and $m=1$, approximately 81° and 74°, respectively, are close to those of the symmetric and antisymmetric wedge cases, approximately 80° and 73°, respectively. Secondly, as can be immediately seen from figure 5, the $m=1$ mode is dominant over the whole range of angles. This implies that, except under special circumstances, the flow near the apex will be determined by this mode no matter what the stirring. In the two-dimensional case, the physical reason for the dominance of the antisymmetric mode is that its field is structurally simpler. A similar argument seems to hold in the conical field. In any case, close to the apex it is the $m=1$ mode that is dominant rather than the axisymmetric $m=0$ mode.

We conclude this section by pointing out the relationship of this field to other internal Stokes flow fields involving sharp corners. Although there are the natural differences that we would expect because of the increase in dimensionality, the conical field is clearly the direct counterpart of the two-dimensional wedge flow considered in Moffatt (1964*a*). As in the two-dimensional case, simple similarity solutions exist, sequences of corner eddies exist for both even and odd m and a critical angle exists beyond which the corner eddies disappear. On the other hand, the situation is quite different for the three-dimensional wedge flows considered in Sano & Hasimoto (1980), Moffatt & Mak (1999) and Shankar (2000). Here there was no simple similarity solution and corner eddies did not exist for symmetric flows, i.e. for even m. This is why it was earlier suggested that the conical flow is the natural extension to three-dimensions of the two-dimensional wedge flow.

2.3. *The flow in a lid-driven cone*

The inner eigenfunctions found in § 2.1 can be used to determine the flow field in a conical container generated by data given on its lid†. For simplicity, let us assume that the lid is the spherical surface at a (dimensional) distance $\tilde{r}_1$ from the apex. If $\tilde{r}_1$ is now chosen as the length scale used for non-dimensionalization, the lid boundary conditions will have to be applied on $r=1$.

Imagine the lid $r=1$ to be moving along its own spherical surface in the x-direction, i.e in a direction parallel to $\phi=0$. Also assume that the speed is of unit magnitude smoothly decaying to 0 at the conical sidewall consistent with (B1*a*). Then the boundary condition on $r=1$ is

$$u_r(1,\theta,\phi)=0, \tag{16a}$$

$$u_\theta(1,\theta,\phi)=\cos\phi\mathscr{F}_1(\theta;\alpha,\delta), \tag{16b}$$

$$u_\phi(1,\theta,\phi)=-\sin\phi\mathscr{F}_1(\theta;\alpha,\delta), \tag{16c}$$

where the function $\mathscr{F}_1(\theta;\alpha,\delta)$ is defined in Appendix B. From (16), it is clear that to represent the field in the cone, we need only use the $m=1$ eigenfunctions in the general representation (12). We therefore expand the velocity field as follows

$$u_r(r,\theta,\phi)=\cos\phi\sum_{j=1}[a_j r^{\mu_j} f_{rj}(\theta;\mu_j)+\mathrm{Re}\{b_j r^{\lambda_j} g_{rj}(\theta;\lambda_j)\}], \tag{17a}$$

$$u_\theta(r,\theta,\phi)=\cos\phi\sum_{j=1}[a_j r^{\mu_j} f_{\theta j}(\theta;\mu_j)+\mathrm{Re}\{b_j r^{\lambda_j} g_{\theta j}(\theta;\lambda_j)\}], \tag{17b}$$

$$u_\phi(r,\theta,\phi)=\sin\phi\sum_{j=1}[a_j r^{\mu_j} f_{\phi j}(\theta;\mu_j)+\mathrm{Re}\{b_j r^{\lambda_j} g_{\phi j}(\theta;\lambda_j)\}], \tag{17c}$$

† Here and hereinafter, all eigenfunction sequences will be assumed to be complete in an appropriate manifold.

https://doi.org/10.1017/S0022112005005458 Published online by Cambridge University Press

where

$$f_{rj}(\theta;\mu_j) = (\mu_j+1)P^1_{\mu_j+1}(\cos\theta) + b(\mu_j-1)\cos\theta P^1_{\mu_j}(\cos\theta), \tag{18a}$$

$$f_{\theta j}(\theta;\mu_j) = P^{1'}_{\mu_j+1}(\cos\theta) + a\frac{2}{\sin\theta}P^1_{\mu_j}(\cos\theta) + b\{\sin\theta P^1_{\mu_j}(\cos\theta) + \cos\theta P^{1'}_{\mu_j}(\cos\theta)\}, \tag{18b}$$

$$f_{\phi j}(\theta;\mu_j) = -\left[\frac{1}{\sin\theta}P^1_{\mu_j+1}(\cos\theta) + 2aP^{1'}_{\mu_j}(\cos\theta) + b\cot\theta P^1_{\mu_j}(\cos\theta)\right], \tag{18c}$$

and identical formulae hold for $g_{rj}(\theta;\lambda_j)$ etc. with the μ_j replaced by λ_j. Note that a and b are still given by (9).

The problem of determining the field in the cone has been reduced to finding the real scalars $\{a_j, j=1,2,\ldots\}$ and the complex scalars $\{b_j, j=1,2,\ldots\}$ such that the boundary conditions on $r=1$ (16*a–c*) are satisfied. It has already been shown in many cases (Shankar 1997, 1998, 2000) that the least total error squared method, or the least-squares method, can be used to easily determine the coefficients in an efficient reliable manner, irrespective of the number of spatial dimensions and geometry and even in unsteady flows (Shankar, Kidambi & Hariharan 2003). We therefore do not describe the method here, but it is outlined in Appendix B. All the detailed results given in this paper, including those shown in figures 2 and 3, have been obtained using this procedure. We postpone their discussion until § 3.

2.4. *The outer eigenfunctions and the flow field in a conical container*

The inner eigenfunctions found in § 2.1 are unbounded as $r\to\infty$; we would expect the existence of outer eigenfunctions that decay at infinity and are unbounded for $r\to 0$. A very natural procedure would be to check whether the characteristic equation (8) has roots with negative real part and calculations quickly confirm their existence. Indeed, Malyuga (2005) has already pointed out the existence of a relationship between the roots with positive real part and those with negative real part: if λ is a root of (8) then so is $-(\lambda+1)$. Calculations quickly suggest the correctness of this relationship, but the result is difficult to prove.

Let λ be a root of (8), i.e. $\mathscr{E}(\lambda)=0$ and consider $\mathscr{E}(-\lambda-1)$. The aim is to show that the latter vanishes. If we make use of the fact that $P^m_{-\lambda-1}=P^m_\lambda$ and $P^m_{-\lambda}=P^m_{\lambda-1}$, we find

$$\mathscr{E}(-\lambda-1) = -\frac{2m^2\cot\alpha}{\sin\alpha}P^{m\,2}_\lambda P^m_{\lambda-1} - \lambda P^m_{\lambda-1}P^{m'}_\lambda\left(\sin\alpha P^m_\lambda + \cos\alpha P^{m'}_\lambda\right) + (\lambda+2)\cos\alpha P^{m'}_{\lambda-1}P^{m'}_\lambda P^m_\lambda. \tag{19}$$

The obvious plan now would be to use the recurrence relations between the spherical harmonics of different degree (see Appendix A) to eliminate $P^m_{\lambda-1}$ in favour of P^m_λ and $P^m_{\lambda+1}$ and then use $\mathscr{E}(\lambda)=0$ to shown that $\mathscr{E}(-\lambda-1)$ vanishes. Although this is simple in principle, the algebra turns out to be excessive. An easier procedure is to note that $B=r^{-\lambda-1}\mathrm{e}^{\mathrm{i}m\phi}P^m_\lambda(\cos\theta)$, $\boldsymbol{A}_1=-r^{\lambda-1}\mathrm{e}^{\mathrm{i}m\phi}\{(m/\sin\theta)P^m_\lambda(\cos\theta)\boldsymbol{e}_\theta+\mathrm{i}P^{m'}_\lambda(\cos\theta)\boldsymbol{e}_\phi\}$ and $\boldsymbol{A}_2=r^{-\lambda-1}\,\mathrm{e}^{\mathrm{i}m\phi}P^m_\lambda(\cos\theta)\boldsymbol{e}_k$ are also solutions of Laplace's equation. If these are used to generate velocity fields through (2*a*) and linearly combined to satisfy the no-slip condition on $\theta=\alpha$, we obtain precisely (19) as the characteristic equation. This proves the result that we were seeking, i.e. if λ is an eigenvalue, then so is $-\lambda-1$. We call the eigenfunctions corresponding to the latter the outer eigenfunctions since they decay for $r\to\infty$; these are once again given by (7) while the scalars a and b are given by (9).

https://doi.org/10.1017/S0022112005005458 Published online by Cambridge University Press

If $\{\mu_j, \boldsymbol{f}_j(\theta;\mu_j)\}$ and $\{\lambda_j, \boldsymbol{g}_j(\theta;\lambda_j)\}$ are the inner eigenvalues and eigenfunctions, we denote the corresponding outer eigenvalues and eigenfunctions by $\{\hat{\mu}_j, \hat{\boldsymbol{f}}_j(\theta;\hat{\mu}_j)\}$ and $\{\hat{\lambda}_j, \hat{\boldsymbol{g}}_j(\theta;\hat{\lambda}_j)\}$; in other words $\hat{\mu}_j = -\mu_j - 1$, etc. With the inner and outer eigenfunctions, it is now possible to determine flow fields in conical containers which do not include the apex. Again, in order to keep matters simple, let us consider conical containers whose upper and lower boundaries are spherical surfaces of radii $\tilde{r}_1$ and $\tilde{r}_0$ with $\tilde{r}_0 < \tilde{r}_1$. Let $\tilde{r}_1$ be chosen as the length scale and assume that data $(\cos m\phi U_{1r}(\theta), \cos m\phi U_{1\theta}(\theta), \sin m\phi U_{1\phi}(\theta))$ be given on $r = 1$ and similar data with U_1 replaced by U_0 be given on $r = r_0 = \tilde{r}_0/\tilde{r}_1$. The following eigenfunction expansions then suggest themselves for the velocity field

$$u_r(r,\theta,\phi) = \cos m\phi \sum_{j=1} \left[\left\{ a_j r^{\mu_j} f_{rj}(\theta;\mu_j) + \hat{a}_j \left(\frac{r}{r_0}\right)^{\hat{\mu}_j} \hat{f}_{rj}(\theta;\hat{\mu}_j) \right\} + \mathrm{Re}\left\{ b_j r^{\lambda_j} g_{rj}(\theta;\lambda_j) + \hat{b}_j \left(\frac{r}{r_0}\right)^{\hat{\lambda}_j} \hat{g}_{rj}(\theta;\hat{\lambda}_j) \right\} \right], \tag{20a}$$

$$u_\theta(r,\theta,\phi) = \cos m\phi \sum_{j=1} \left[\left\{ a_j r^{\mu_j} f_{\theta j}(\theta;\mu_j) + \hat{a}_j \left(\frac{r}{r_0}\right)^{\hat{\mu}_j} \hat{f}_{\theta j}(\theta;\hat{\mu}_j) \right\} + \mathrm{Re}\left\{ b_j r^{\lambda_j} g_{\theta j}(\theta;\lambda_j) + \hat{b}_j \left(\frac{r}{r_0}\right)^{\hat{\lambda}_j} \hat{g}_{\theta j}(\theta;\hat{\lambda}_j) \right\} \right], \tag{20b}$$

$$u_\phi(r,\theta,\phi) = \sin m\phi \sum_{j=1} \left[\left\{ a_j r^{\mu_j} f_{\phi j}(\theta;\mu_j) + \hat{a}_j \left(\frac{r}{r_0}\right)^{\hat{\mu}_j} \hat{f}_{\phi j}(\theta;\hat{\mu}_j) \right\} + \mathrm{Re}\left\{ b_j r^{\lambda_j} g_{\phi j}(\theta;\lambda_j) + \hat{b}_j \left(\frac{r}{r_0}\right)^{\hat{\lambda}_j} \hat{g}_{\phi j}(\theta;\hat{\lambda}_j) \right\} \right], \tag{20c}$$

and the problem is now to determine the two real sequences $\{a_j\}$ and $\{\hat{a}_j\}$ and the two complex sequences $\{b_j\}$ and $\{\hat{b}_j\}$ from the given data on $r = 1$ and $r = r_0$. However this is easily done using the least-squares procedure described in Appendix B.

3. A discussion of the flow fields

We will now briefly discuss the flow fields that are generated in the cone and in the conical container when data is prescribed on the lid. In all of the calculations, the number of eigenfunctions used N, i.e. the finite upper limit of all the sums shown in the expansions (17) and (20), was 50, while M, the number of equidistant least-squares minimization points (see Appendix B), was $2N$. Thus, there are 150 real scalars to be found in the case of the cone and 300 in the case of the conical container. All the usual checks to make sure of the accuracy of the field at the boundaries were made; the use of the functions $\mathscr{F}_1$ and $\mathscr{F}_2$, which are smooth and compatible with symmetry and the sidewall conditions, permits rapid convergence of the series to the correct data.

Figure 2 shows, for various cone half-angles, the streamline patterns in the symmetry plane of a cone when $m = 1$. In all calculations, the parameter δ which appears in the definition of $\mathscr{F}_1$ and $\mathscr{F}_2$ was taken to be 0.05α; note that the radial extent is $0 < r < 1$ in all the panels. The most striking feature in the figure is the large number of eddies seen when the cone angle is small, 10°, and the reduction in the number of eddies seen as the cone angle is increased. Recall that the dimensions of the eddies fall off as $r \to 0$ in a geometrical progression with common ratio e^{π/q_1}, where $\lambda_1 = p_1 + iq_1$.

https://doi.org/10.1017/S0022112005005458 Published online by Cambridge University Press

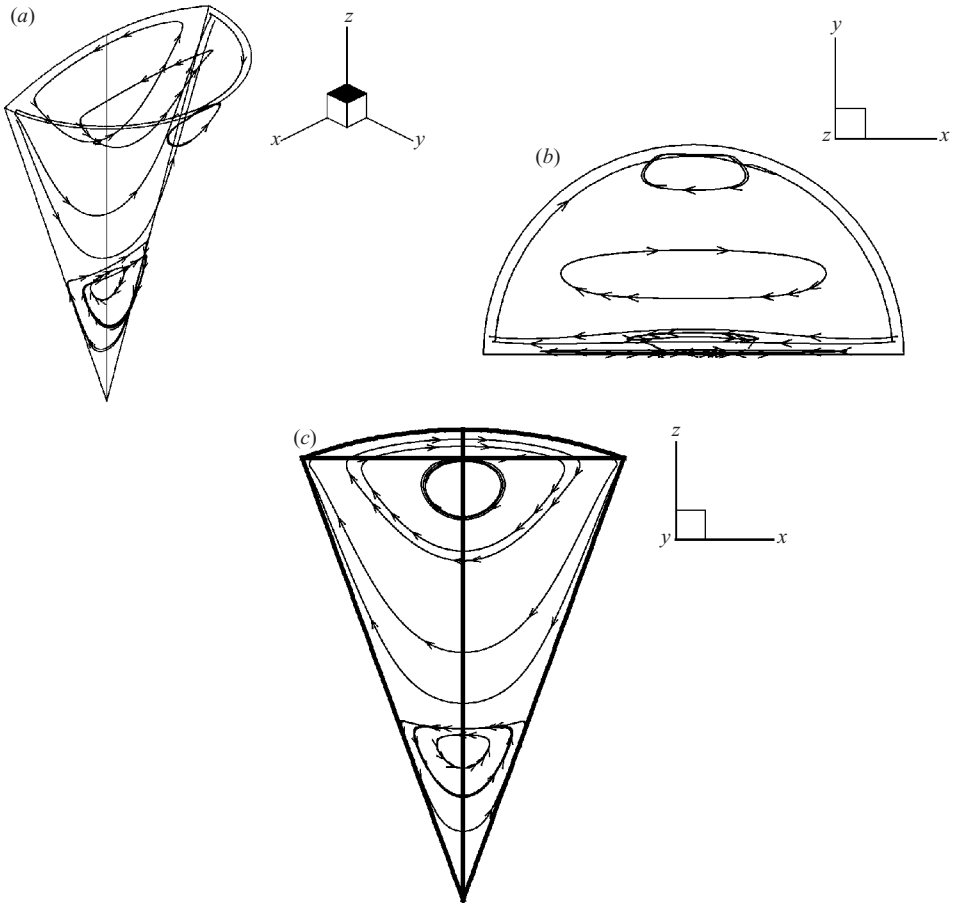


FIGURE 6. Three-dimensional streamline patterns in a cone of half-angle $\alpha = 20°$; only half the cone is shown. $m = 1$. (*a*) Streamlines seen in perspective, (*b*) the plan view of the streamlines and (*c*) as seen in the y-direction.

Examining table 1, it may be noted, that q_1 decreases from about 6.37 to 1.14 as α increases from 10° to 45°; this qualitatively explains the relative eddy size ratios that are seen. The three-dimensional streamline patterns corresponding to the $\alpha = 20°$ case are shown in figure 6. All streamlines appear to be closed, as they have to be under the imposed symmetries, with an increasing tendency to bend as they are displaced away from the plane $\phi = 0$. In each eddy, these streamlines move about a stagnation line that connects one side of the conical wall to the other. Especially to be noted is the streamline that moves azimuthally near the top rim, from near $\phi = \pi$ to $\phi = 0$, before taking part in the general downward motion near $\phi = 0$. The second and third eddy (not shown), have similar features, but without the azimuthal motion.

A comparison of the principal eigenvalues in the case of the cone with the corresponding ones for the two-dimensional wedge show that they are close over a range of apex angles. For example for $\alpha = 20°$, they are approximately $6.934 + 3.098\mathrm{i}$ and $7.058 + 3.095\mathrm{i}$, respectively. This raises the question of how similar the flow field in the symmetry plane of the cone is to the corresponding two-dimensional field generated by the principal wedge eigenvalue. These fields are compared in figure 7, where the eight streamlines in figure 7(*a*) are those in the symmetry plane of figure 6.

https://doi.org/10.1017/S0022112005005458 Published online by Cambridge University Press

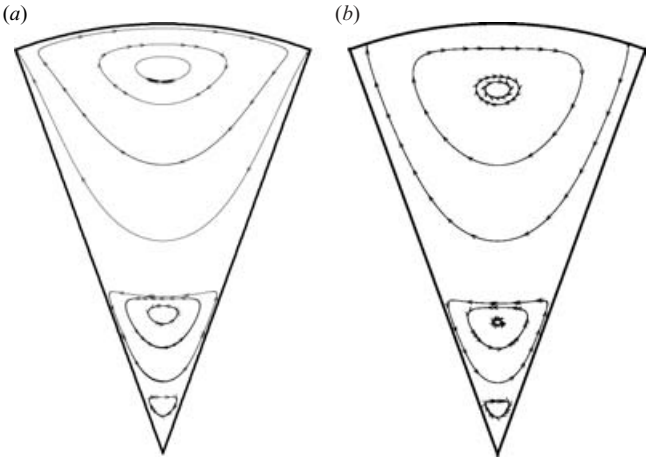


FIGURE 7. A comparison of the streamlines of figure 6 in the symmetry plane $\phi = 0, \pi$ with those derived from an appropriately scaled two-dimensional wedge field generated by the dominant wedge eigenvalue. (*a*) The three-dimensional field in this plane, (*b*) the two-dimensional field.

The field in figure 7(*b*) is the appropriately scaled two-dimensional field with the streamlines that go through the same eight lowest points of those in figure 7(*a*). The second and third eddies look very similar. Not unexpectedly, although the streamlines well below the primary eddy centres are similar, near the top the two fields are very different. Naturally, the enforcement of the no-slip condition at the lid generates fields that differ, with the contributions of the other eigenvalues becoming important.

The $m = 2$ case is considered in figure 3. Here the conditions on the lid are similar to (16), but with ϕ replaced by 2ϕ and $\mathscr{F}_1$ replaced by $\mathscr{F}_2$. The reason for the latter change is that symmetry about the plane $\theta = \pi/2$ requires v_θ to vanish at the polar axis, a condition that $\mathscr{F}_2$ satisfies but $\mathscr{F}_1$ does not. Note that the $m = 2$ field is symmetric about both $\phi = 0$ and $\phi = \pi/2$ and antisymmetric about $\phi = \pi/4$. All streamlines are closed with the polar axis being a stagnation line; for each eddy there is a stagnation line, connecting the polar axis to the cone, about which the closed streamlines make their circuits. As noted earlier, only the streamlines in the symmetry planes are planar and they move from points on the polar axis to other points on the polar axis.

Figure 8 shows a typical flow field in a conical container when $\alpha = 20^\circ$ and $r_0 = 0.35$ with the same lid data, (16), as used for the cones and no-slip on the bottom wall. Figure 8(*a*) may be compared with figure 2(*b*). The chief novelty here is the existence of corner eddies along the bottom corner. It may be noted that, in this case, the bottom corner is formed by two surfaces neither of which is planar, and little is known about flows in such neighbourhoods. Whereas the streamlines, apart from the corner eddy, are quite similar to those seen in the conical container, there does not seem to be any azimuthal flow of the type seen in figure 6. As in the case of the cylinder (Shankar 1997), the bottom eddy consists in the symmetry plane of two foci with streamlines going from one to the other and an azimuthal flow from one to the other, away from this plane.

From figure 2(*b*), we would guess that as r_0 is decreased from 0.35, the corner eddy will increase in size, touch and merge to form a new primary eddy (Shankar 1997). This process is shown in figure 9. When $r_0 = 0.32$, the situation is much like at

https://doi.org/10.1017/S0022112005005458 Published online by Cambridge University Press

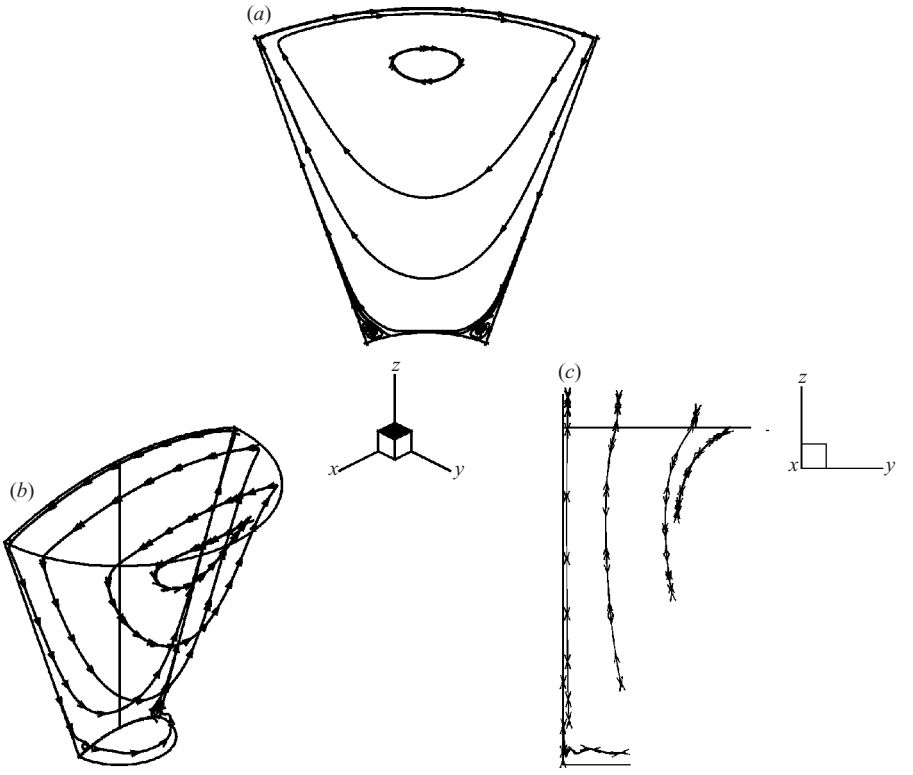


FIGURE 8. Slow viscous flow in a conical container whose top and bottom walls are spherical surfaces. $m = 1, \alpha = 20°, r_0 = 0.35$. (*a*) Streamlines in the plane of symmetry $\phi = 0, \pi$, (*b*) some three-dimensional streamlines and (*c*) a side view of these three-dimensional streamlines.

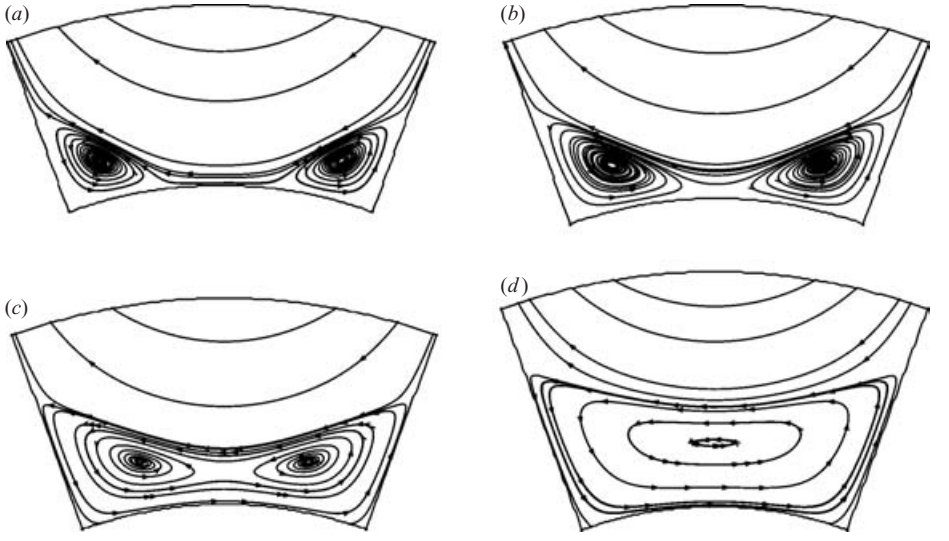


FIGURE 9. Streamlines in the symmetry plane for flow in a conical container, $m = 1, \alpha = 20°$. The radial region shown in each case is $r_0 < r < 0.45$. (*a*) $r_0 = 0.32$, (*b*) 0.31, (*c*) 0.30 and (*d*) 0.28.

https://doi.org/10.1017/S0022112005005458 Published online by Cambridge University Press

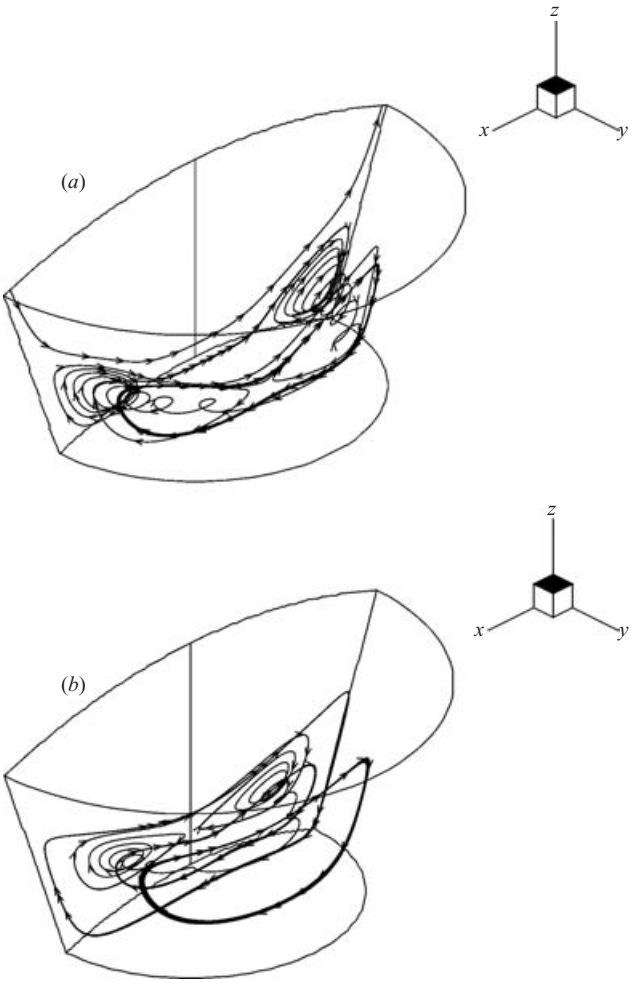


FIGURE 10. Three-dimensional streamline patterns in the radial region $r_0 < r < 0.45$ associated with the flows considered in figures 9(a) and 9(c), respectively.

$r_0 = 0.35$, but the corner eddy is much larger. When $r_0 = 0.31$, the opposite segments have already touched and there are now streamlines which go from one focus to the other by the short route across the polar axis. The toroidal structure has lifted off from the bottom and is contained in the nascent second primary eddy in figure 9(c) when $r_0 = 0.30$; and it is not visible at all in figure 9(d) when $r_0 = 0.28$. No new corner eddy is visible, most probably because of our inadequate resolution. Three-dimensional streamline patterns corresponding to the cases in figures 9(a) and 9(c) are shown in figure 10. These are very similar to the toroidal corner eddies that were observed in Shankar (1997) and it appears that the curvature of the bottom does not change things much.

Finally, we wish to consider a case where $\alpha > 90°$. This would correspond to flow past a conical obstacle contained in a spherical container; when r_0 is not zero, the obstacle would have a part of a sphere attached to it. The situation is illustrated in figure 11 when $\alpha = 160°$. The first five real and complex eigenvalues are given in table 1. The principal eigenvalue is real and so we do not expect any corner eddies

https://doi.org/10.1017/S0022112005005458 Published online by Cambridge University Press

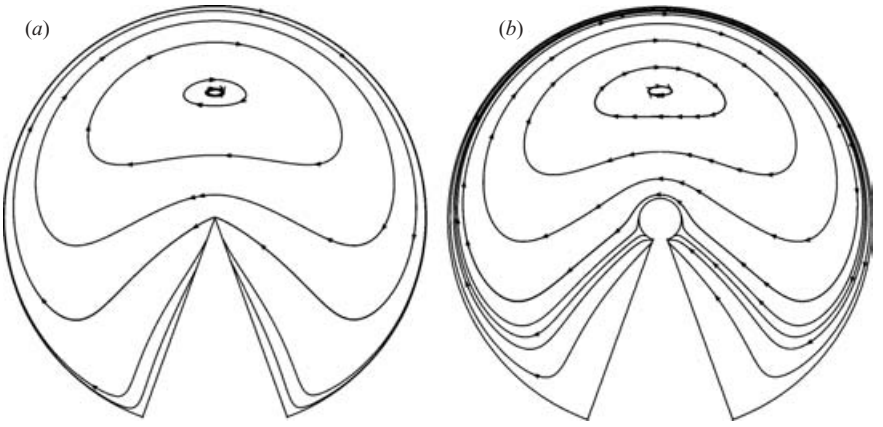


FIGURE 11. External flows past conical objects in a spherical container. $\alpha = 160°$, $m = 1$. (*a*) Flow past a cone and (*b*) flow past a cone topped by a sphere, $r_0 = 0.1$.

at the apex; the lid data are once again given by (16). Figure 11(*a*) shows that, as expected there is a general circulation consistent with the lid motion with a stagnation line well above the cone apex. This picture is not changed much when the cone has a part of a sphere, with $r_0 = 0.1$, attached to its top. Once again we emphasize that complex eigenvalues very much play a role here, but the dominant one is real.

4. Conclusion

We have shown that similarity solutions exist for the conical geometry which, apart from the mathematical complexity, very much resemble those for the two-dimensional wedge found by Moffatt (1964*a*). Since these involve complex eigenvalues, the argument given by Moffatt applies and it is found that corner eddies will in general exist at the vertex for both even and odd wavenumbers m, provided $\alpha < \alpha^*$. In this, the cone-vertex field is somewhat different from the three-dimensional wedge type fields (Sano & Hasimoto 1980; Moffatt & Mak 1999; Shankar 2000), where it appears that corner eddy sequences do not exist for even m.

Assuming the set of similarity solutions to be complete, they can be used to calculate the field in a finite cone where data is given on the upper lid of the cone. On the other hand, if one needs to compute the field in a conical container, i.e. one which does not contain the vertex of the cone, one will also need in addition the set of outer eigenfunctions. It was shown that the outer eigenvalues can be obtained from the inner ones and hence that the flow in a conical container can be written down as an eigenfunction expansion. Examples were given of flow field calculations based on such expansions with the coefficients determined by the least squares procedure. The principal features of these flows that were elucidated were the dependence of the eddy structure on the cone angle and the merger of the corner eddy in a container to form the new primary eddy as the container length increased.

I would like to thank Professor O. Sano for recently bringing to my attention the paper by Kim (1979), where in the special case of the motion of a sphere in the neighbourhood of the vertex of a cone, the existence of an infinite sequence of eddies in its neighbourhood is demonstrated. I would also like to thank the referees for a number of helpful suggestions.

https://doi.org/10.1017/S0022112005005458 Published online by Cambridge University Press

Appendix A

We collect here a number of useful formulae pertaining to the associated Legendre function $P_\nu^m(x)$ for integer $m \geqslant 0$, $-1 < x < 1$ and ν an arbitrary complex number. For more details, see Lebedev (1972). $P_\nu^m(x)$ is a solution of the ordinary differential equation

$$(1-x^2)\frac{\mathrm{d}^2u}{\mathrm{d}x^2} - 2x\frac{\mathrm{d}u}{\mathrm{d}x} + \left[\nu(\nu+1) - \frac{m^2}{1-x^2}\right]u = 0, \tag{A 1}$$

and has the following representation in terms of the hypergeometric function:

$$P_\nu^m(x) = \frac{(-1)^m\Gamma(\nu+m+1)}{2^m\Gamma(m+1)\Gamma(\nu-m+1)}(1-x^2)^{m/2}F\left(m-\nu,\nu+m+1;m+1;\tfrac{1}{2}(1-x)\right). \tag{A 2}$$

The following relations hold:

$$(x^2-1)\frac{\mathrm{d}P_\nu^m(x)}{\mathrm{d}x} = \nu x P_\nu^m(x) - (\nu+m)P_{\nu-1}^m(x), \tag{A 3a}$$

$$(\nu-m+1)P_{\nu+1}^m(x) - (2\nu+1)xP_\nu^m(x) + (\nu+m)P_{\nu-1}^m(x) = 0, \tag{A 3b}$$

$$P_{-\nu-1}^m(x) = P_\nu^m(x). \tag{A 3c}$$

For most of the calculations described in this paper, the following integral representation was used:

$$P_\nu^m(\cos\beta) = \frac{(-1)^m 2\Gamma(\nu+m+1)}{\sqrt{\pi}\Gamma\left(m+\frac{1}{2}\right)\Gamma(\nu-m+1)}\frac{1}{(2\sin\beta)^m} \times \int_0^\beta \frac{\cos\left(\nu+\frac{1}{2}\right)\theta}{(2\cos\theta-2\cos\beta)^{1/2-m}}\mathrm{d}\theta \quad (0<\beta<\pi). \tag{A 4}$$

Since the integrand is either (integrably) singular or non-analytic near $\theta = \beta$, the integral in this neighbourhood was evaluated analytically, accurate to high order using *Mathematica*, and added to the numerical integral over the rest of the interval. In this manner, $P_\nu^m(\cos\beta)$ could be evaluated very accurately even when $|\nu|$ was very large.

Appendix B

The purpose of this Appendix is to define the two functions $\mathscr{F}_1(\theta;\alpha,\delta)$ and $\mathscr{F}_2(\theta;\alpha,\delta)$ that were used in §§ 2.3 and 2.4 and to outline the method of least squares that is used to determine the unknown coefficients in expansions of the type (12).

We define the two functions on $[0,\alpha]$ which have been used in the main text

$$\mathscr{F}_1(\theta;\alpha,\delta) = \begin{cases} 1 & (0 \leqslant \theta \leqslant (\alpha-\delta)), \\ 0.5\{1+\cos[\pi(\theta-(\alpha-\delta))/\delta]\} & ((\alpha-\delta) < \theta \leqslant \alpha), \end{cases} \tag{B 1a}$$

$$\mathscr{F}_2(\theta;\alpha,\delta) = \begin{cases} \dfrac{1}{2}\left\{1+\cos\left(\dfrac{\pi(\theta-\delta)}{\delta}\right)\right\} & (0 \leqslant \theta < \delta), \\ 1 & (\delta \leqslant \theta \leqslant (\alpha-\delta)), \\ 0.5\{1+\cos[\pi(\theta-(\alpha-\delta))/\delta]\} & ((\alpha-\delta) < \theta \leqslant \alpha). \end{cases} \tag{B 1b}$$

If δ is small, $\mathscr{F}_1(\theta;\alpha,\delta)$ is just equal to 1 over most of the interval and then falls smoothly to 0 near the endpoint; $\mathscr{F}_2(\theta;\alpha,\delta)$ is similar to $\mathscr{F}_1$, but also falls smoothly to 0 at the origin.

https://doi.org/10.1017/S0022112005005458 Published online by Cambridge University Press

We now outline the least-squares procedure for the case of flow in the cone considered in § 2.3. Assume that N eigenfunctions are used and let $(U_r(\theta), U_\theta(\theta), U_\phi(\theta))$ denote any set of admissible prescribed boundary conditions such as (16) with the ϕ dependence factored out. Divide the interval $[\epsilon, \alpha]$ into M equal intervals where ϵ is a small quantity, of the order of 10^{-4} and call the equidistant points θ_k, $k = 1, 2, \ldots, M$. Using (17), we can define the errors e_{1k}, e_{2k} and e_{3k} in satisfying the three boundary conditions at each such point as follows

$$e_{1k} = -U_r(\theta_k) + \sum_{j=1}^{N} [a_j f_{rj}(\theta_k) + \mathrm{Re}\{b_j g_{rj}(\theta_k)\}], \tag{B 2a}$$

$$e_{2k} = -U_\theta(\theta_k) + \sum_{j=1}^{N} [a_j f_{\theta j}(\theta_k) + \mathrm{Re}\{b_j g_{\theta j}(\theta_k)\}], \tag{B 2b}$$

$$e_{3k} = -U_\phi(\theta_k) + \sum_{j=1}^{N} [a_j f_{\phi j}(\theta_k) + \mathrm{Re}\{b_j g_{\phi j}(\theta_k)\}], \tag{B 2c}$$

and the total error squared as

$$E^2 = \sum_{k=1}^{M} \{e_{1k}^2 + e_{2k}^2 + e_{3k}^2\}. \tag{B 3}$$

If now E^2 is minimized with respect to the $3N$ real scalars $\{a_1, b_1^r, b_1^i, \ldots, a_N, b_N^r, b_N^i\}$, we obtain a system of $3N$ linear equations from which the scalars can be determined. We expect, and experience shows, that as $N, M \to \infty$, the coefficients tend to converge to limiting values.

REFERENCES

Hills, C. P. & Moffatt, H. K. 2000 Rotary honing: a variant of the Taylor paint-scraper problem. *J. Fluid Mech.* **418**, 119–135.

Imai, I. 1973 *Ryutai Rikigaku* (*Fluid Mechanics*), vol 1. Syokabo, Tokyo [in Japanese].

Kim, M.-U. 1979 Slow viscous flow due to the motion of a sphere on the axis of a circular cone. *J. Phys. Soc. Japan* **47**, 1670–1675.

Lebedev, N. N. 1972 *Special Functions and their Applications*. Dover.

Liu, C. H. & Joseph, D. D. 1978 Stokes flow in conical trenches. *SIAM J. Appl. Maths* **34**, 286–296.

Malyuga, V. S. 2005 Viscous eddies in a circular cone. *J. Fluid Mech.* **522**, 101–116.

Meleshko, V. V., Malyuga, V. S. & Gomilko, A. M. 2000 Steady Stokes flow in a finite cylinder. *Proc. R. Soc.* A **456**, 1741–1758.

Moffatt, H. K. 1964*a* Viscous and resistive eddies near a sharp corner. *J. Fluid Mech.* **18**, 1–118.

Moffatt, H. K. 1964*b* Viscous eddies near a sharp corner. *Arch. Mech. Stosow.* **2**, 365–372.

Moffatt, H. K. & Duffy, B. R. 1980 Local similarity solutions and thier limitations. *J. Fluid Mech.* **96**, 299–313.

Moffatt, H. K. & Mak, V. 1999 Corner singularities in three-dimensional Stokes flow. *IUTAM Symp. on Non-Linear Singularities in Deformation and Flow*, 21. Kluwer.

Morse, P. M. & Feshbach, H. 1953 *Methods of Theoretical Physics*, part 2. McGraw-Hill.

Sano, O. & Hasimoto, H. 1980 Three-dimensional Moffatt-type eddies due to a Stokeslet in a corner. *J. Phys. Soc. Japan* **48**, 1763–1768.

Shankar, P. N. 1997 Three-dimensional eddy structure in a cylindrical container. *J. Fluid Mech.* **342**, 97–118.

Shankar, P. N. 1998 Three-dimensional Stokes flow in a cylindrical container. *Phys. Fluids* **10**, 540–549.

Shankar, P. N. 2000 On Stokes flow in a semi-infinite wedge. *J. Fluid Mech.* **422**, 69–90.

https://doi.org/10.1017/S0022112005005458 Published online by Cambridge University Press

Shankar, P. N., Kidambi, R. & Hariharan, J. 2003 Oscillatory eddy structure in a container. *J. Fluid Mech.* **494**, 163–185.

Tran-Cong, T. & Blake, J. R. 1982 General solution of the Stokes' flow equations. *J. Math. Anal. Appl.* **90**, 72–84.

Wakiya, S. 1976 Axisymmetric flow of a viscous fluid near the vertex of a body. *J. Fluid Mech.* **78**, 737–747.

Weidman, P. D. & Calmidi, V. 1999 Instantaneous Stokes flow in a conical apex aligned with gravity and bounded by a stress-free surface. *SIAM J. Appl. Maths* **59**, 1520–1531.

https://doi.org/10.1017/S0022112005005458 Published online by Cambridge University Press